

**Universidade do Minho**  
Escola de Ciências



***Essay: Lead-free multiferroic heterostructures for enhanced magnetic field sensing***

Tiago Rodrigues, id11777

Prof. Bernardo Almeida

April 2025

## Table of content

1.	Introduction .....	3
2.	State-of-the-art .....	4
2.1.	Multiferroic magnetoelectric composite materials .....	4
2.1.1.	Multiferroic magnetoelectric materials .....	4
2.1.2.	Magnetoelectric composites .....	5
2.2.	Magnetic Sensors .....	7
2.3.	Laser Ablation.....	11
2.3.1.	Procedure .....	11
2.3.2.	Influence of deposition parameters .....	13
2.3.3.	Advantages and disadvantages .....	14
3.	Research Proposal.....	16
3.1.	Objectives.....	16
3.2.	Work Plan.....	16
3.3.	Research proposal timeline .....	19
4.	References .....	21

## **1. Introduction**

This essay aims to provide a theoretical and bibliographical basis to the PhD project named “Lead-free multiferroic heterostructures for enhanced magnetic field sensing”, which aims to develop piezoelectric-magnetostrictive multiferroic magnetoelectric (ME) nanocomposite bilayer, multilayer and/or vertically aligned systems based on selected combinations of lead-free high piezoelectricity compounds such as BCZT, KNN or BNT-BT, combined with high magnetostriction materials (ferrites, CM compounds), for enhanced magnetic sensing.

Thin film ME magnetic sensors have been poorly explored and their small size and in-plane anisotropy are essential for spatially resolved, vector magnetic field or sensor array measurements. By using high magnetostriction/piezoelectricity materials, the non-linear characteristics of the magnetostriction curve and/or a piezoelectric-induced periodic actuation, then arbitrary frequencies outside resonance are transferred to the mechanical resonance amplifying the dynamic ME signal. With vertically aligned clamp-free structures, further ME enhancements are achieved.

Thus, the planned study aims to deepen the understanding of the electromechanical, dielectric, magnetic and dynamical magnetoelectric properties of composites at the nanoscale and to develop highly sensitive, miniaturized and biocompatible sensors for magnetic field detection.

## 2. State-of-the-art

Artificial strain coupled magnetolectric (ME) composites [1]–[9], containing magnetostrictive and piezoelectric materials, where the magnetic (electric) field can be detected/controlled electrically (magnetically), have been the subject of much scientific and technological interest. The exhibited strong ME coupling (as high as  $\sim 21\text{Vcm-Oe}^{-1}$  in BaTiO<sub>3</sub>/BiFeO<sub>3</sub> films [9]) arises from the mechanical interaction between both phases and the electric, magnetic and elastic fields all couple together. Thus, they have potential for applications in information storage, sensors, actuators, antennas and low power energy efficient electronics. [3]–[9]. In this section, their properties and applications will be further discussed.

### 2.1. Multiferroic magnetolectric composite materials

#### 2.1.1. Multiferroic magnetolectric materials

Figure 1 illustrates the relationship between the magnetolectric, multiferroic materials and the quantities involved.[10]

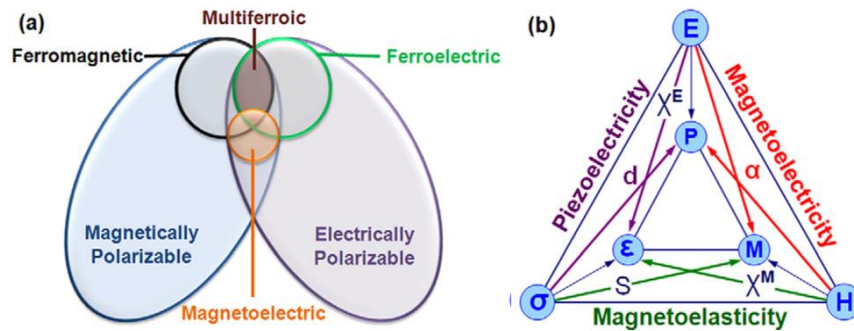


**Figure 1-** Relationship between magnetolectric and multiferroic materials. b) Diagram of the different types of coupling present in the materials. It is emphasized the materials with a coupling of the electric and magnetic orders, denominated by magnetolectric materials.[10]

As observed, magnetolectric multiferroic materials exhibit a coupling between their magnetic and electrical properties. This coupling means that applying an electric field can influence the material's magnetization, while a magnetic field can shift its electrical polarization. The strength of this magnetolectric response is captured by the magnetolectric coefficient,  $\alpha$ , defined as:[11], [12]

$$\alpha = \frac{\partial E}{\partial H}$$

where E is the electric field and H is the applied magnetic field.

Single-phase, or intrinsic, magnetolectric materials typically show modest magnetolectric coefficients, often tied to their weak polarizations or magnetizations. Conventional multiferroic oxides like BiFeO<sub>3</sub> and YMnO<sub>3</sub>, known their robust spontaneous polarization, have low magnetolectric (ME) coupling.[13], [14] Stronger couplings are expected to emerge in electronic ferroelectrics, such as those with charge-ordered. Yet, their small polarization values and low Curie temperatures keep them from being practical.[15], [16]

On top of that, the magnetic or electrical ordering in these materials usually disappears well below room temperature, vastly limiting their viability in real-world applications. As a solution to this problem, composite materials were theorized, showing great promise and versatility.

### 2.1.2. Magnetoelectric composites

As stated, the combination of a ferromagnetic (magnetostrictive) material and a ferroelectric (piezoelectric) material results in a magnetoelectric composite due to the mechanical coupling between the phases.[17] The possibility to choose different phase materials has opened the door to testing all many magnetoelectric composites, playing with different setups and structures. These composites result in multiferroic materials with impressive magnetization and polarization, plus a strong magnetoelectric (ME) coupling that holds up at room temperature.

By combining a magnetostrictive phase with a piezoelectric one through strain-mediated coupling, it is possible to obtain a magnetoelectric effect, through the process shown in Figure 2. When acting with a magnetic field on the material, the magnetostrictive phase responds by deforming and, thanks to elastic coupling, that deformation will also occur on the piezoelectric phase, creating an electric polarization (P). The same process will also happen in reverse order: an applied electric field will stress the piezoelectric phase, which will deform the magnetostrictive phase, originating a magnetization (M).

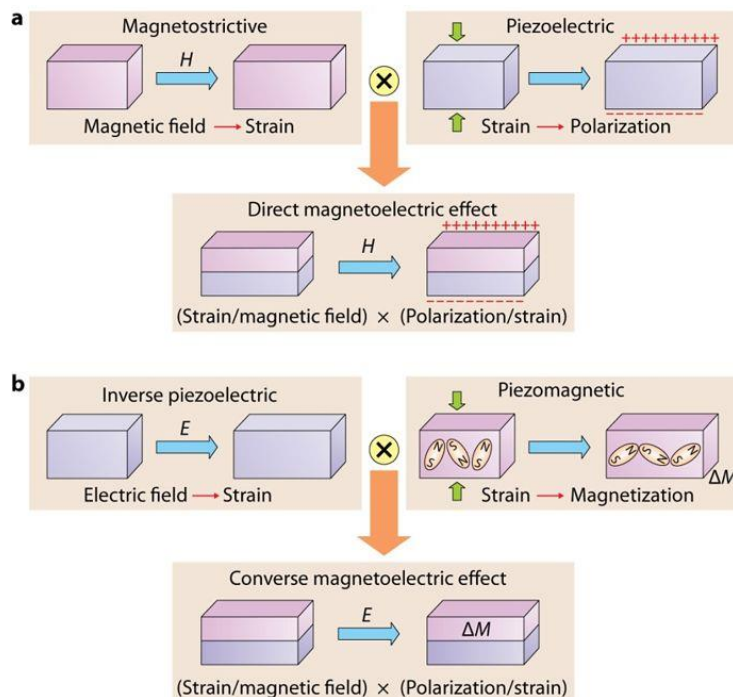


**Figure 2:** Schematic illustration of strain-mediated ME effect in a composite system consisting of a magnetic layer (purple) and ferroelectric layer (pink). (a) Direct ME effect: an in-plane magnetic field,  $H$  induces strain in the magnetic component due to the magnetostrictive effect, which is mechanically transferred to the ferroelectric component inducing a dielectric polarization through the piezoelectric effect. (b) Converse ME effect: an out-of-plane electric field,  $E$  induces strain in the ferroelectric component due to the inverse piezoelectric effect, which is mechanically transferred to the magnetic component, inducing a magnetization change,  $\Delta M$  or domain reorientation through the piezomagnetic effect. [18]

Artificial ME multiferroics combining ferroelectric and ferromagnetic phases have been developed as an alternative to single-phase ME materials showing enhancements in the ME performance.[19]–[21] The obtained magnetoelectric composites allow to produce materials with magnetoelectric coefficients up to 100 times higher than the corresponding intrinsic magnetoelectric ones, depending on their geometry and component phases.

The coupling geometry of the phases can be varied, resulting in composite materials with different characteristics. Newnham proposed a notation (0-3, 1-3 and 2-2) capable of describing the two-phase composite structure by connecting one material to another, as shown in Figure 3. They correspond to:

- 0–3: Integrated particles of one material within another material;
- 1–3: Pillars of one material within another;
- 2–2: Materials connect to surfaces in thin or multilayer films.

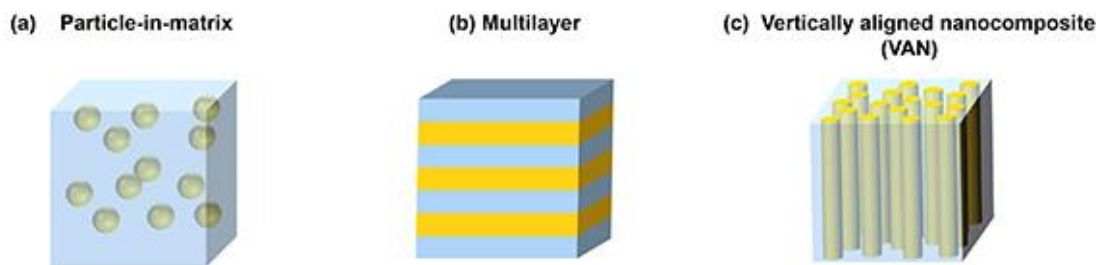


**Figure 3**-Schematic illustration of three kinds of ME composite nanostructures with common connectivity schemes: (a) 0-3 particulate nanocomposite films with magnetic particles (0) embedded in a ferroelectric film matrix (3); (b) 2-2 horizontal heterostructure with alternating ferroelectric (2) and magnetic (2) layers, or simply a ferroelectric (or magnetic) thin film grown on a magnetic (or ferroelectric) substrate; and (c) 1-3 vertical heterostructure with one-phase nanopillars (1) embedded in a matrix of another phase (3) [22]

Nevertheless, such multilayer heterostructures require demanding and costly production techniques, interfaces tend to be leaky and their speeds are apt to be slow since their elastic coupling is limited by the speed of sound (due to the ferroelectric domain wall propagation speed).

## 2.2. Magnetic Sensors

Magnetic sensors have many applications, including magnetic storage, navigation systems, robotics or medical sensors, such as magnetosensitive eskins magnetoencephalography and magnetocardiography.[5]–[7], [23]–[25]

Magnetic field sensors based on Superconducting Quantum Interference Devices (SQUIDs) stand out for their high sensitivity, with a detection limit of  $5 \text{ fT}/\text{Hz}^{1/2}$  at 4.2 K for a 1 Hz magnetic signal. That precision makes them invaluable for applications in areas like medical imaging or geophysical exploration. However, these devices depend on cryogenic cooling systems, usually liquid helium, to sense magnetic fields, which make typical SQUID setups not just expensive to buy and run, but also bulky.[26]

On the other hand, Hall effect and magnetoresistive sensors don't need extreme cooling, relying instead on changes in voltage or resistance to detect magnetic fields, which makes them go-to options for applications at room temperature. Their weakness, however, is their considerable power consumption usually needed to deliver decent sensitivity, and the required hefty electronics to sift through noise and process signals[26]

Another alternative in magnetic sensing devices are fluxgate sensors and magneto-optic sensors, who also present some challenges. Fluxgate sensors, with high reliability in navigation or space missions, tend to be physically bulky, making their application in tight space devices cumbersome. Magneto-optic sensors, on the other hand, make use of the Faraday effect, shifting light polarization to measure magnetic fields, showing high degrees of precision. But they often demand detailed optical alignment procedures, that require high vigilance to maintain the reliability of the device. [26]

It is clear to see, then, that all these options—SQUIDs, Hall, magnetoresistive, fluxgate, and magneto-optic sensors—have all incredible strengths that allow them to shine in specific applications, failing, however, to present a solution with high flexibility for different applications. None quite cracks the code for a perfect blend of sensitivity, cost, and simplicity.

On the other hand, piezoelectric-magnetostrictive composite ME magnetic sensors are an appealing alternative, leveraging the coupling between piezoelectric and magnetostrictive materials to detect magnetic fields, with high sensitivity.[5]–[7], [23], [27]–[29] They do not require cooling/heating components, can function in a broad temperature range, including room temperature. This temperature resilience stems from the inherent stability of their constituent materials as piezoelectrics like PMN-PT maintain their electromechanical properties over wide thermal spans, while magnetostrictive alloys like Metglas exhibit consistent magnetic behavior. Furthermore, because these composites are typically insulating, they dissipate ultrasmall amounts of Joule heat during operation. This energy efficiency makes them ideal for applications where power consumption is a critical concern, such as portable medical diagnostics or remote environmental monitoring.

For detailed ME sensing, frequency-conversion approaches [23] or the delta-E effect [30] are employed. These dynamic ME effects and their improvement by mechanical resonances have received little attention in thin film form [18], and frequency dependent studies, such as impedance spectroscopy [19], are needed. Additionally, new materials and material geometries/combinations need to be developed and tested.

In the ongoing search for superior magnetic field sensors, piezoelectric-magnetostrictive composite ME sensors have emerged as a particularly attractive alternative [5-7,10,14-16]. These sensors stand out because they operate without the need for cumbersome cooling or heating systems, function effectively across a wide temperature range—including room temperature—and consume remarkably little power, thanks to their insulating nature, which keeps Joule heating to a minimum.

To unlock their full potential, researchers employ sophisticated techniques like frequency-conversion approaches [10] or the delta-E effect [17]. In frequency-conversion methods, the sensor is excited at one frequency (often near its mechanical resonance), and the ME response is detected at a shifted frequency. This approach exploits nonlinear interactions within the composite to amplify weak signals, making it particularly effective for low-frequency magnetic fields, such as those encountered in geomagnetic studies. The delta-E effect, meanwhile, refers to the magnetic-field-induced change in the elastic modulus of the magnetostrictive phase. This change shifts the composite's resonance frequency, providing a measurable signature of the applied field.

However, these dynamic ME effects—especially when enhanced by mechanical resonances—remain underexplored in thin film form.[31] Thin films, typically deposited on substrates like silicon or glass, face unique constraints: the substrate can clamp the in-plane strain, reducing the ME coupling efficiency. Additionally, the reduced dimensions alter the resonance frequencies and damping characteristics, necessitating new design strategies. For instance, tailoring the film thickness or introducing stress-relief layers could mitigate these issues, but such approaches remain underexplored. There's a clear need for more in-depth investigations, such as impedance spectroscopy [32], to shed light on their frequency-dependent behavior. Through impedance spectroscopy, it is possible to study the resonance behavior of a material, identifying damping losses, and highlighting the frequency bands where the ME response is strongest. For example, a peak in the impedance spectrum might indicate the fundamental resonance mode, giving essential information for the tuning of the sensor's operating frequency, for maximum sensitivity. Such studies could also inform the design of multilayered thin films, where alternating piezoelectric and magnetostrictive layers enhance the interfacial coupling. Moreover, the field is ripe for innovation in material geometries and combinations, which could push the boundaries of what these sensors can achieve.

The best ME sensors reported so far were bulk-like Metglas/PMN-PT piezofiber structures, with a detection limit of  $5.1 \text{ pT}/\text{Hz}^{1/2}$  for 1 Hz magnetic field, rivaling some SQUID sensors.[23] The success of this design lies in its architecture, where thin Metglas foils are bonded to PMN-PT fibers, ensuring efficient

strain transfer across a large surface area. The fibers, often aligned unidirectionally, amplify the piezoelectric response, while Metglas's high magnetic permeability concentrates the field-induced strain.

However, ME magnetic sensors in thin-film form are preferable, since their small size is essential for spatially resolved measurements or for sensor arrays.[24], [25] In addition, with their in-plane anisotropy, vector magnetic field measurements are achieved. For instance, by orienting two thin-film sensors perpendicularly, researchers can resolve both the magnitude and direction of the field, a capability invaluable for navigation systems or geophysical surveys. By using vertically aligned composites, which are free from substrate clamping [33], the ME response is further enhanced. In these structures, since the magnetostrictive and piezoelectric phases are stacked perpendicularly to the substrate, the strain propagates in the out-of-plane direction rather than being constrained in-plane. This configuration enhances the ME response by preserving the full mechanical freedom of the composite.

For environmental friendly and biocompatible applications, lead-free piezoelectrics [20], such as BCZT ((1-x)(Ba<sub>0.7</sub>Ca<sub>0.3</sub>TiO<sub>3</sub>)-x[Ba(Zr<sub>0.2</sub>Ti<sub>0.8</sub>)O<sub>3</sub>] [34], [35], KNN ((K<sub>0.5</sub>Na<sub>0.5</sub>)NbO<sub>3</sub>) [36], [37] and BNT-BT ((Bi<sub>0.5</sub>Na<sub>0.5</sub>)TiO<sub>3</sub>) [38], are favorable for ME sensors as they present high piezoelectric coefficients (496 [34], 250 [36], 190 [38] pC/N), comparable to the state-of-the-art PZT ceramics, along with high dielectric constant and low losses. They have been poorly explored for high performance ME thin film sensing. Figure 4 shows the temperature dependence of the dielectric constant and loss of BCZT, as well as its cubic perovskite structure.[39] At its core, BCZT's appeal lies in its perovskite lattice, a versatile structure that mirrors the cubic perovskite structure (ABO<sub>3</sub>) of BaTiO<sub>3</sub>, with a tailored composition of calcium (Ca<sup>2+</sup>) partially replacing barium at the A-site, and zirconium (Zr<sup>4+</sup>) replacing titanium at the B-site. These substitutions reshape the lattice into a supercell configuration (often modeled as a 5 × 2 × 2 array for computational studies), introducing subtle distortions that profoundly enhance the material's properties. These lattice substitutions create a morphotropic phase boundary, where ferroelectric phases, specifically rhombohedral and tetragonal, coexist in a delicate balance. At this boundary, the energy barriers between these phases become remarkably low, allowing the lattice to shift quickly in response to an electric field. The zirconium plays a key role in amplifying the ferroelectric polarization through larger ionic shifts, while calcium lends structural resilience, keeping the material reliable across a wide range of temperatures.

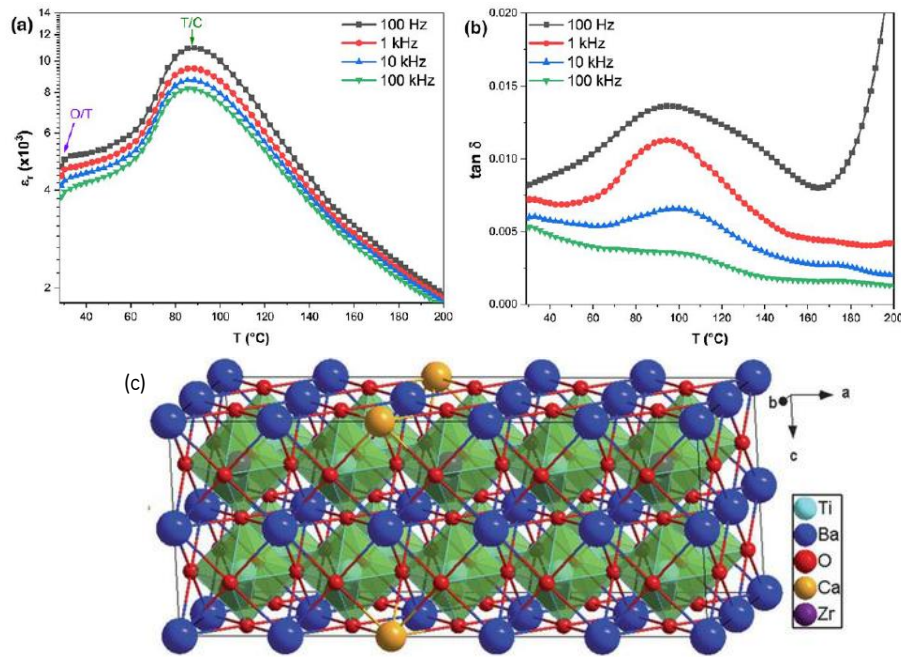


**Figure 4** Temperature-dependence of the (a) dielectric constant and (b) dielectric loss of  $Ba_{1-x}Ca_xZr_yTi_{1-y}O_3$  (BCZT) ceramic at different frequencies. O/T corresponds to orthorhombic–tetragonal transition and T/C denotes the tetragonal–cubic phase transition. (c) Cubic perovskite structure and arrangements of atoms in a  $B_{0.98}C_{0.02}Zr_{0.15}T_{0.85}O_3$  supercell with  $5 \times 2 \times 2$  dimension. [39]

The selected magnetic phase materials include (Ni,Co)Fe<sub>2</sub>O<sub>4</sub> ferrites, with high magnetocrystalline anisotropy and magnetostriction and NiMnGa and La(Fe,Si), compounds that present colossal magnetostriction (CM).[40]–[43]. The magnetostriction coefficient of the ferrites, enables significant strain generation under modest magnetic fields, making them reliable components in ME sensors and actuators. Their high Curie temperatures further ensure thermal stability of the composite material.

The CM materials have magnetostrictions one order of magnitude higher than best-known conventional ones, thus, having potential to form highly sensitive films. In NiMnGa, the high magnetostrictive behavior stems from martensitic phase transformations triggered by magnetic fields, where the lattice reorients to produce macroscopic deformation.[41] In La(Fe,Si) the CM effect is driven by magnetovolume transitions, where the lattice expands significantly due to spin-lattice coupling.[43]

Taking advantage of the high piezoelectric and magnetostrictive properties of the chosen materials further enhancements of ME magnetic sensing are achieved, as dynamic effects depend on them. As such, their inclusion in ME thin films will then allow developing miniaturized, lightweight, biocompatible sensors for biomagnetic and high sensitivity magnetic field detection.[44]

For the preparation of nanostructured thin films, laser ablation is a strong candidate, since it allows creating high-quality epitaxial films, due to the high kinetic energy of the plume particles and permits the congruent transfer of the bulk target material onto the nanostructures, with the preservation of their stoichiometry. It then appears as a highly favorable deposition technique to prepare the envisaged thin films.

### 2.3. Laser Ablation

For thin film production, pulsed laser deposition (PLD), a physical vapor deposition (PVD) technique, is widely used due to its advantages comparatively to other PVD techniques, as it is based on vaporizing the target with a high-powered pulsed laser. A scheme of typical PLD equipment is present in Figure 5. As observed, the substrate is placed inside an ultra-high vacuum chamber on a holder that can potentially be heated. The substrate temperature is measured as close as possible to the center of the substrate.

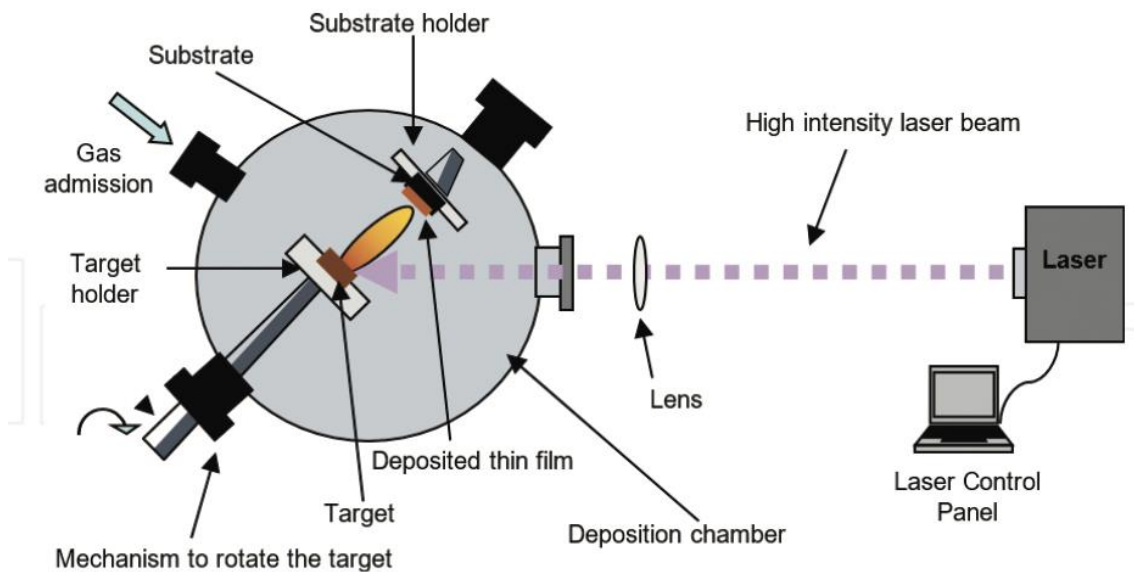


**Figure 5-** Experimental set-up for laser ablation

#### 2.3.1. Procedure

The main process of laser ablation can be described of a rapid cycle between 3 phases that repeats continuously: vaporization of the target material after interaction with the laser, transport of the resulting material plume towards the substrate, and growth of the thin film on the surface of the substrate.

The deposition process begins with the removal of material from a constantly rotating target, as depicted in Figure 5, through a high-powered pulsed laser directed at the target material, which causes rapid heating that leads to localized melting vaporization. [45] A schematic of the process of target vaporization is depicted in Figure 6.

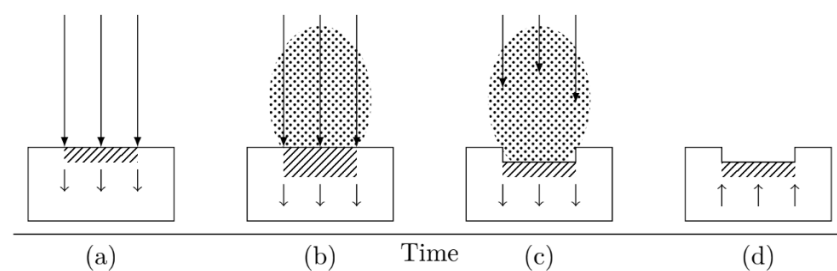


**Figure 6-** Schematic of the ablation process. (a) Initial absorption of the radiation (long arrows) and target melting (shaded area, short arrows indicate the motion of solid-liquid interface). (b) Heat flow spreads through the target, leading to its vaporization and

*formation of a plume. (c) Vaporization continuous and the radiation interacts with the plume, prompting the formation of a plasma. (d) Target cooling and solidification. [45]*

The target is continuously exposed to the pulsed laser beam with typical time per pulse of  $\sim 25$  ns. Since the laser's energy is delivered in such a brief period, the target's temperature increases very fast too, resulting in the material being ejected from the target through mechanisms such as vaporization, boiling, and even explosive boiling, and the emission of particles ranging from the nanoscale to the microscale.[46] The emitted material can, itself, be the desired deposition material or a precursor that reacts with a background reactive gas inside the chamber that will then form the desired film.

The heating of the target surface, thus, plays a crucial role in the ablation process and can either be initiated directly by the interaction with the laser pulse, or indirectly by the recoil pressure produced when material is ablated at the beginning of the pulse. As the vaporization starts, the accompanying latent heat of the process results in a cooling effect to the surface, while not interfering with the temperature of the material right below it. This continuous subsurface heating, usually at depths lower than the optical penetration depth of the laser, leads to an explosion of solid material on the surface, due to the difference in temperature between it and the material underneath it. The explosion generates a plasma plume that is highly directed forward and highly congruent to the target material.[47]

This plume is made up of ejected ions and atoms, from all the elements present in the target, keeping roughly the same stoichiometric proportions as the original material and is, then, rapidly irradiated by the laser pulses, which get absorbed.[48] The absorption, logically, occurs mostly in areas packed with charged particles, which are usually right near the bulk target surface.[49] This results in the excitation and ionization of the species in the plume, and a weakening of the laser light that reaches the target, past the interaction with the plume.[45], [46]

While the plume initially shoots out in one direction, it starts expanding in all three directions through adiabatic processes, propelled by collisions with the background gas and interactions within the plume itself.[45]–[47] While, in a vacuum, the plume's shape and velocity would eventually level off to steady values over time, in the presence of a background gas, the propagation of the plume is slowed down and stalled after a few microseconds, with the propagation velocity being determined from the interaction between the ions in the plume and the background gas atoms and molecules in the chamber. [46], [50], [51]

Once those plume particles hit the substrate, they diffuse on the surface and form chemical bonds, resulting in the growth of a thin film.[52] The film's morphology will be dependent on some factors, namely the kinetic energy of the incoming plume particles, the substrate's temperature, the deposition rate, the probability of adhesion of the particles on the substrate surface, and the lattice mismatch between the substrate and the film itself.[53] Therefore, the film's properties and quality come down to a range of deposition parameters that can be controlled: the substrate type and temperature, the laser's wavelength,

pulse duration, and intensity, and the use or not of a background gas.[45] Once the laser pulse ends, the target quickly cools down, with solidification of the material and the gradual recession of the melt front, as depicted on Figure .

### 2.3.2. Influence of deposition parameters

As discussed, the deposition of thin films and the quality of the film is influenced by several factors. Of special importance are: the temperature, the parameters of the laser at the base pressure and the selected target/substrate.

#### Temperature

The temperature of the substrate is one of the determining factors in the growth of high-quality thin films. Films deposited on room-temperature substrates usually turn out amorphous, while their crystallinity improves with the increase in substrate temperature.[45] Pairing high substrate temperatures with slow deposition rates also enables epitaxial growth and higher crystallinity, by letting adatoms roam across the surface until they lock into stable lattice positions. [53]. On the flip side, thin films deposited at low temperatures or high rates tend to stay amorphous.

Figure 7 shows the influence of substrate temperature on the quality and crystallinity of the film.[54] The structure of the film will depend on the substrate temperature,  $T_S$ , relative to the target's melting temperature,  $T_M$ . When  $T_S$  is less than 0.3-times  $T_M$ , the films have a granular look with no visible epitaxial growth. However, when  $T_S$  falls between 0.3- and 0.5-times  $T_M$ , columnar structures are promoted, and the film has epitaxial growth. With  $T_S$  above 0.5- times  $T_M$ , the film starts forming grains bigger than its own thickness, leading to build up tension between these oversized grains, that eventually cracks the film.

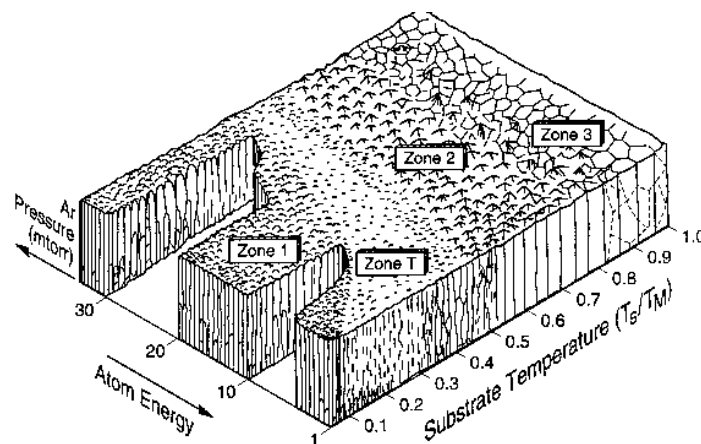


**Figure 7-** Thornton diagram showing the relation between microstructure of PVD thin films and temperature and pressure during deposition. [54]

#### Laser parameters

The growth of thin films is significantly influenced by the fluence, wavelength, and repetition rate of the laser beam. While longer wavelengths enhance the penetration depth of the laser pulse into the target

material, allowing, consequently, deeper interaction with the subsurface layers, shorter wavelengths, with their reduced penetration, yield films that exhibit greater homogeneity and fewer surface particulates, as the ablation process is more confined.

As previously noted, laser fluence stands out as a critical parameter in the deposition process. Increasing fluency concentrates more energy per unit area onto the target, generating a plume populated with highly energetic particles. The greater kinetic energy of these particles promotes epitaxial growth, due to the higher mobility of the adatoms, whereas particles with lower energy tend to favor amorphous growth. In general, an increase in fluence also results in an acceleration of the ablation rate. However, this acceleration isn't always beneficial, as it can lead to a shielding effect where the plume absorbs most of the laser radiation, thereby reducing the efficiency of material removal from the target.

The pulse repetition rate adds another layer of complexity for the choice of laser parameters. Higher repetition rates, and consequently higher deposition rates, tend to produce films with a more amorphous structure and smaller grain sizes, while lower rates permit the conditions for epitaxial growth, allowing adatoms sufficient time to settle into ordered lattice positions. However, at a fixed fluence, lower frequencies permit excess laser energy to dissipate thermally into the target, reducing overall efficiency of the process. Conversely, increasing the repetition rate minimizes this thermal loss by delivering pulses in rapid succession, enhancing the ablation efficiency and elevating the deposition rate.

Therefore, it is necessary to carefully consider and select the laser parameters for each deposition, in order to obtain the best balance between efficiency of the process and the quality of the film.

### **2.3.3. Advantages and disadvantages**

Laser ablation, as a deposition technique, brings a blend of strengths and weaknesses to the table, showcasing both its power and its challenges in thin film fabrication. Its advantages stand out in a few key ways:

- The wavelength and fluence of the laser offer a lot of flexibility, allowing fine-tuning of the deposition process according to the target material being used.
- Sharp control over the film growth rate, which is vital for materials with exact thicknesses or structures required.
- Congruent transfer of material from the target to the film, holding onto stoichiometry even for more complex compositions.
- Adjustable kinetic energy of the ejected particles, through laser parameters and gas pressure, allowing control of the growth of the film.

However, there are also some disadvantages to point out:

- The kinetic energy of the ejected particles needs to be closely controlled, as, with high enough energy, it's possible to create re-pulverization of material and damage to the deposited film.

- The distribution of laser pulse energy isn't homogeneous, resulting in the plume having an angular energy spread, and films with thickness that varies across the substrate. This factor represents a big limitation in the maximum size of sample that can be produced.
- Possible presence of particulates (ranging from 1 nm to several  $\mu\text{m}$ ) on the film, often due to explosive boiling or splashing of molten target material. Lowering the laser fluence below the explosive boiling threshold—either by cutting energy or widening the laser spot—helps reduce this effect. Techniques like target rotation or rastering the laser across the surface also minimize droplets by letting the target solidify between pulses.[14]

Despite the few limitations of the technique, laser ablation presents some great strengths to deposit the pretended materials, especially the stoichiometric transfer of material from a complex target to a film on a substrate and the capacity to produce epitaxial layers in a simple form. Exact values for substrate temperature, gas pressure, and laser parameters need to be studied to guarantee high-quality, replicable samples.

### **3. Research Proposal**

#### **3.1. Objectives**

The project aims to explore the dynamical magnetoelectric properties of multiferroic nanocomposite films based on selected combinations of leadfree high piezoelectricity compounds such as BCZT, KNN or BNT-BT, combined with high magnetostriction materials (ferrites, CM compounds), for enhanced magnetic sensing. Although, single-phase magnetoelectrics can function as magnetic field sensors, this has been impractical, as their Curie temperatures are below room temperature. On the other hand, composite systems have higher ME responses and broader alternatives, as the selection of the active phases is wider and less stringent. Additionally, the strain tuning and control of the coupled magnetic-electric dynamical ME behavior is further achieved through interface engineering. Thus, combining lead-free high piezoelectricity and magnetostriction compounds allows building coupled electricmagnetic miniaturized, lightweight, biocompatible thin film sensors aiming for detection limits  $<1 \text{ pT/Hz}^{1/2}$  to low-frequency ( $10^{-2}$  to  $10^3$  Hz) magnetic fields.

The specific objectives are:

1. Synthesis of laser ablated (10nm-200 nm) thin films composed by epitaxial piezoelectric/magnetostrictive bilayers/multilayers and vertically aligned composites. Systematic characterization of their structural, chemical and morphological properties. Of particular relevance is to study and tailor phase/phase and phase/substrate interface structures towards improving the interface engineered strain coupling.
2. Systematic characterization of the magnetic properties as a function of temperature and magnetic field. Study of the type of magnetic ordering, critical temperatures and the influence of interfacial strain.
3. Systematic characterizations of the frequency dependent electric properties and relaxation behavior (impedance spectroscopy, P-E hysteresis cycles) of the films. Determination of the influence of strain on the onset of polar order, critical temperatures and coercive fields.
4. Studies of dynamical electric field/magnetic field induced coupled magnetic and electric responses. Characterization of the interplay between the local interfacial structure and the magnetic and electric behavior, towards attaining new coupled lead-free dynamic electric-magnetic multifunctionalized nanocomposites for magnetic field sensing.

#### **3.2. Work Plan**

The work plan will be supported by ongoing research projects (2022.03564.PTDC, M-ERA-NET3/0003/2021), in the field of magnetoelectric materials, related to the proposed studies. It will also take advantage of ongoing national and international collaborations of the members of the research teams involved. Here, the work plan is divided in several, complementary parts:

### 1. Deposition and processing of the nanostructures

In this part of the work thin film heterostructures (bylayers/multilayers/vertically-aligned) composed by lead-free BCZT  $((1-x)(\text{Ba}_{0.7}\text{Ca}_{0.3}\text{TiO}_3)-x[\text{Ba}(\text{Zr}_{0.2}\text{Ti}_{0.8})\text{O}_3])$ , KNN  $((\text{K}_{0.5}\text{Na}_{0.5})\text{NbO}_3)$  or BNT-BT  $((\text{Bi}_{0.5}\text{Na}_{0.5})\text{TiO}_3)$  compounds and high magnetostriction (Co,Ni)-ferrites and NiMnGa or La(Fe,Si) colossal magnetostriction materials will be deposited at different gas pressures (oxygen, argon) and substrate temperatures. The depositions will be made by pulsed laser ablation at CFUM, using an excimer laser with wavelength of 248 nm. Post-deposition annealing of the films will be done, if needed to induce proper crystalline phases or create phase-segregation in the vertically aligned structures. By choosing selected

crystalline substrates, such as Si/Pt, SrTiO<sub>3</sub>, SrTiO<sub>3</sub>:Nb, LaAlO<sub>3</sub> or MgO that are known to improve epitaxial growth of the layers, controlled traction or compression can be further applied to the films depending on their lattice mismatch with substrate. Several series of samples will be made with different layer thicknesses and growth orientations in order to study their interface structure and dielectric, magnetic, magnetoelectric and ME sensing properties.

### 2. Structural, chemical and spectroscopic analysis

This part of the work involves the structural and chemical characterization of the films and of the ablation targets. The studies will occur simultaneously and in close connection with the films deposition part. Of particular relevance is the characterization of the phase/phase and phase/substrate interfaces structure, particularly important to attain epitaxial growth and strain coupling in the films. The structural characterization will be performed by X-ray diffraction, using the facilities at CFUM and SEMAT-Minho. The X-ray diffraction measurements will allow determining the crystallinity and phases present in the films, as well as preferential growth directions. The microstructure and surface characterization of the films will be performed by scanning electron microscopy (SEM) and atomic force microscopy (AFM). Chemical characterization will be done by Energy Dispersive X-ray analysis (EDX). Raman and infrared reflectivity measurements will be performed to gather complementary information on the structural and chemical properties of the films, including the presence of polar modes.

### 3. Study of the electric properties of the films

The dielectric studies, along with the magnetic measurements, will be particularly important to understand the magnetoelectric behaviour of the films and to select samples with optimized ME responses. A systematic characterization will be made for the different chosen lead-free piezoelectrics, their layer thicknesses and combinations with the magnetostrictive component. The objective is to access their electrical and dielectric dynamic (AC) response to the applied electric fields.

A detailed quantitative analysis by broadband impedance spectroscopy can separate the leakage, inhomogeneity and parasite capacitance effects, and shed light on the intrinsic ME coupling mechanisms. As such, these experiments will provide valuable information about the nature of the strain coupling and induced polarizations, influencing the electrical and magnetic properties of the system. The work involves

the determination of the complex dielectric constant of the films by impedance spectroscopy, as a function of temperature and frequency at CFUM. A closed cycle cryostat and an oven combined with an impedance analyzer will be used for temperature dependent measurements, covering the range 20-570K. The frequency region is 10Hz-3GHz. The measurements will allow determining relaxation phenomena and lattice phase transition temperatures (including ferroelectric Curie temperatures) for the lead free piezoelectric materials. Also, the determination of electrical polarization P-E hysteresis cycles, at different temperatures, will be performed to check the existence of ferroelectric order and to obtain spontaneous and remnant polarizations, coercive field and switching behaviour.

#### 4. Study of the magnetic properties of the films

A systematic characterization of the magnetization behaviour of the thin films will be performed, in the temperature range 4-500K, for the different magnetostrictive layer compositions and thicknesses. Magnetic hysteresis cycles will also be measured at selected temperatures, with magnetic fields up to 5.5 Tesla. The magnetic measurements will be done using the SQUID magnetometer of IFIMUP. Magneto-optical Kerr effect (MOKE) measurements will be performed using the facilities at CFUM and IFIMUP, as a function of temperature (15-300K) and magnetic field (up to 1Tesla). Of particular importance is the determination of the type of magnetic ordering (superparamagnetism, ferrimagnetism, spin-glass behavior) of the multiferroic heterostructures, and to the determination of the critical temperatures related to the magnetic behaviour of the films.

#### 5. Study of the coupled magnetoelectric and magnetic field sensing properties of the films

From the previous results, selected groups of samples presenting magnetic and electric order indicative of the existence of a stress mediated coupling between the lead-free piezoelectric and magnetostrictive phases, will be measured at CFUM and IFIMUP in order to determine their magnetoelectric properties, dynamic ME behavior and magnetic sensing characteristics. It involves the determination of the complex dielectric permittivity and polarization under an applied magnetic field and the behaviour of the magnetization under an applied electric field. Dynamic frequency dependent magneto-impedance spectroscopy measurements, particularly near resonances, is envisaged. For dynamic ME magnetic sensing studies, frequency-conversion approaches will be used, taking advantage of the non-linear characteristics of the magnetostriction curve or a piezoelectric-induced periodic actuation of the sensor. They allow transferring an arbitrary frequency outside resonance to the mechanical resonance frequency of the sensor amplifying the response signal. These combined studies will then allow obtaining a deeper knowledge on the role of the stress mediated coupling between the piezoelectric and magnetostrictive materials responsible for the onset of multiferroic behaviour in the films. They will also allow to take advantage of the dynamic ME behaviour to develop new coupled magnetic-electric multifunctionalized nanocomposite systems for magnetic sensing.

### **3.3. Research proposal timeline**

The proposed timeline to complete the project is presented in Figure 8. As stated in Section 3.2, the experimental phase of this project begins with the deposition and processing of the nanostructures through laser ablation, testing different phase combinations and architectures. Following the fabrication stage, comprehensive characterization including structural, chemical, spectroscopic, electric and magnetic analysis analyses will be performed to further examine the resulting materials, as well as allowing for an understanding of their properties and an optimization of the produced materials. For the final goal, the coupled magnetoelectric and magnetic field sensing properties of the films will be tested and optimized, leading to a deeper knowledge on the role of the stress-mediated coupling between the piezoelectric and magnetostrictive materials on the onset of multiferroic behaviour in the films and the proposal of new highly-optimized coupled magnetic-electric multifunctionalized nanocomposite systems for magnetic sensing.



## 4. References

- [1] N. A. Spaldin and R. Ramesh, "Advances in magnetoelectric multiferroics," *Nat. Mater.*, vol. 18, no. 3, pp. 203–212, 2019, doi: 10.1038/s41563-018-0275-2.
- [2] N. A. Spaldin, "Multiferroics beyond electric-field control of magnetism.," *Proceedings. Math. Phys. Eng. Sci.*, vol. 476, no. 2233, p. 20190542, Jan. 2020, doi: 10.1098/rspa.2019.0542.
- [3] S. Shevlin, "Multiferroics and the path to the market," *Nat. Mater.*, vol. 18, no. 3, pp. 191–192, 2019, doi: 10.1038/s41563-019-0295-6.
- [4] C. Leung, J. Li, D. Viehland, and X. Zhuang, "A review on applications of magnetoelectric composites: from Heterostructural uncooled magnetic sensors, Energy harvesters to Highly efficient power converters," *J. Phys. D: Appl. Phys.*, vol. 51, Jun. 2018, doi: 10.1088/1361-6463/aac60b.
- [5] S. Kopyl, R. Surmenev, M. Surmeneva, Y. Fetisov, and A. Kholkin, "Magnetoelectric effect: principles and applications in biology and medicine– a review," *Mater. Today Bio*, vol. 12, p. 100149, 2021, doi: <https://doi.org/10.1016/j.mtbio.2021.100149>.
- [6] M. Bichurin *et al.*, "Magnetoelectric Magnetic Field Sensors: A Review," *Sensors*, vol. 21, no. 18, 2021. doi: 10.3390/s21186232.
- [7] S. Zuo *et al.*, "Ultrasensitive Magnetoelectric Sensing System for Pico-Tesla MagnetoMyography," *IEEE Trans. Biomed. Circuits Syst.*, vol. 14, no. 5, pp. 971–984, 2020, doi: 10.1109/TBCAS.2020.2998290.
- [8] M. Ghidini *et al.*, "Shear-strain-mediated magnetoelectric effects revealed by imaging.," *Nat. Mater.*, vol. 18, no. 8, pp. 840–845, Aug. 2019, doi: 10.1038/s41563-019-0374-8.
- [9] D. Gupta and R. K. Kotnala, "A review on current status and mechanisms of room-temperature magnetoelectric coupling in multiferroics for device applications," *J. Mater. Sci.*, vol. 57, pp. 1–28, Jul. 2022, doi: 10.1007/s10853-022-07377-4.
- [10] L. W. Martin *et al.*, "Multiferroics and magnetoelectrics: thin films and nanostructures," *J. Phys. Condens. Matter*, vol. 20, no. 43, p. 434220, 2008, doi: 10.1088/0953-8984/20/43/434220.
- [11] M. Vopsaroiu *et al.*, "Experimental determination of the magnetoelectric coupling coefficient via piezoelectric measurements," *Meas. Sci. Technol.*, vol. 19, no. 4, p. 45106, 2008, doi: 10.1088/0957-0233/19/4/045106.
- [12] W. Eerenstein, N. D. Mathur, and J. F. Scott, "Multiferroic and magnetoelectric materials," *Nature*, vol. 442, no. 7104, pp. 759–765, 2006, doi: 10.1038/nature05023.
- [13] C. N. R. Rao, A. Sundaresan, and R. Saha, "Multiferroic and Magnetoelectric Oxides: The

- Emerging Scenario," *J. Phys. Chem. Lett.*, vol. 3, no. 16, pp. 2237–2246, Aug. 2012, doi: 10.1021/jz300688b.
- [14] T. Zhao *et al.*, "Electrical control of antiferromagnetic domains in multiferroic BiFeO<sub>3</sub> films at room temperature," *Nat. Mater.*, vol. 5, no. 10, pp. 823–829, 2006, doi: 10.1038/nmat1731.
- [15] S. Ishihara, "Electronic Ferroelectricity and Frustration," *J. Phys. Soc. Japan*, vol. 79, no. 1, p. 11010, Jan. 2010, doi: 10.1143/JPSJ.79.011010.
- [16] A. M. L. Lopes, J. P. Araújo, V. S. Amaral, J. G. Correia, Y. Tomioka, and Y. Tokura, "New Phase Transition in the  $\text{Pr}_{1-x}\text{Ca}_x\text{MnO}_3$  System: Evidence for Electrical Polarization in Charge Ordered Manganites," *Phys. Rev. Lett.*, vol. 100, no. 15, p. 155702, 2008, doi: 10.1103/PhysRevLett.100.155702.
- [17] M. Fiebig, T. Lottermoser, D. Meier, and M. Trassin, "The evolution of multiferroics," *Nat. Rev. Mater.*, vol. 1, p. 16046, Jul. 2016, doi: 10.1038/natrevmats.2016.46.
- [18] Y. Wang, J. Hu, Y. Lin, and C.-W. Nan, "Multiferroic magnetoelectric composite nanostructures," *NPG Asia Mater.*, vol. 2, no. 2, pp. 61–68, 2010, doi: 10.1038/asiamat.2010.32.
- [19] V. Garcia, M. Bibes, and A. Barthélémy, "Artificial multiferroic heterostructures for an electric control of magnetic properties," *Comptes Rendus Phys.*, vol. 16, no. 2, pp. 168–181, 2015, doi: <https://doi.org/10.1016/j.crhy.2015.01.007>.
- [20] Y. Zhang, C. Deng, J. Ma, Y. Lin, and C.-W. Nan, "Enhancement in magnetoelectric response in CoFe<sub>2</sub>O<sub>4</sub>–BaTiO<sub>3</sub> heterostructure," *Appl. Phys. Lett.*, vol. 92, no. 6, p. 62911, Feb. 2008, doi: 10.1063/1.2841048.
- [21] A. T. Mulder, N. A. Benedek, J. M. Rondinelli, and C. J. Fennie, "Turning ABO<sub>3</sub> Antiferroelectrics into Ferroelectrics: Design Rules for Practical Rotation-Driven Ferroelectricity in Double Perovskites and A<sub>3</sub>B<sub>2</sub>O<sub>7</sub> Ruddlesden-Popper Compounds," *Adv. Funct. Mater.*, vol. 23, no. 38, pp. 4810–4820, 2013, doi: <https://doi.org/10.1002/adfm.201300210>.
- [22] J. Song and H. Wang, "A material design guideline for self-assembled vertically aligned nanocomposite thin films," *J. Phys. Mater.*, vol. 8, Jan. 2025, doi: 10.1088/2515-7639/ad9bee.
- [23] D. Viehland, M. Wuttig, J. Mccord, and E. Quandt, "Magnetoelectric magnetic field sensors," *MRS Bull.*, vol. 43, pp. 834–840, Nov. 2018, doi: 10.1557/mrs.2018.261.
- [24] J. Hoffmann, E. Elzenheimer, C. Bald, C. Hansen, W. Maetzler, and G. Schmidt, "Active Magnetoelectric Motion Sensing: Examining Performance Metrics with an Experimental Setup," *Sensors*, vol. 21, no. 23. 2021. doi: 10.3390/s21238000.
- [25] C. Becker *et al.*, "A new dimension for magnetosensitive e-skins: active matrix integrated micro-origami sensor arrays," *Nat. Commun.*, vol. 13, no. 1, p. 2121, 2022, doi: 10.1038/s41467-022-29802-7.
- [26] A. Grosz, M. Haji-Sheikh, and S. C. Mukhopadhyay, *High Sensitivity Magnetometers*, vol. 19.

2016. doi: 10.1007/978-3-319-34070-8.
- [27] M. Zaeimbashi *et al.*, "Ultra-compact dual-band smart NEMS magnetoelectric antennas for simultaneous wireless energy harvesting and magnetic field sensing," *Nat. Commun.*, vol. 12, no. 1, p. 3141, 2021, doi: 10.1038/s41467-021-23256-z.
- [28] J. Reermann *et al.*, "Evaluation of magnetoelectric sensor systems for cardiological applications," *Measurement*, vol. 116, pp. 230–238, 2018, doi: <https://doi.org/10.1016/j.measurement.2017.09.047>.
- [29] E. Elzenheimer *et al.*, "Investigation of Converse Magnetoelectric Thin-Film Sensors for Magnetocardiography," *IEEE Sens. J.*, vol. 23, no. 6, pp. 5660–5669, 2023, doi: 10.1109/JSEN.2023.3237910.
- [30] B. Spetzler *et al.*, "Magnetoelastic Coupling and Delta-E Effect in Magnetoelectric Torsion Mode Resonators," *Sensors*, vol. 21, no. 6. 2021. doi: 10.3390/s21062022.
- [31] S. O. Sayedaghaee, C. Paillard, S. Prosandeev, B. Xu, and L. Bellaiche, "Strain-induced resonances in the dynamical quadratic magnetoelectric response of multiferroics," *npj Comput. Mater.*, vol. 6, no. 1, p. 60, 2020, doi: 10.1038/s41524-020-0311-z.
- [32] W. Bai *et al.*, "Dielectric behaviors of Aurivillius Bi5Ti3Fe0.5Cr0.5O15 multiferroic polycrystals: Determining the intrinsic magnetoelectric responses by impedance spectroscopy," *Sci. Rep.*, vol. 5, no. 1, p. 17846, 2015, doi: 10.1038/srep17846.
- [33] R. Wu *et al.*, "Design of a Vertical Composite Thin Film System with Ultralow Leakage To Yield Large Converse Magnetoelectric Effect," *ACS Appl. Mater. Interfaces*, vol. 10, no. 21, pp. 18237–18245, May 2018, doi: 10.1021/acsami.8b03837.
- [34] X. Ji *et al.*, "Structure and electrical properties of BCZT ceramics derived from microwave-assisted sol–gel-hydrothermal synthesized powders," *Sci. Rep.*, vol. 10, no. 1, p. 20352, 2020, doi: 10.1038/s41598-020-73784-9.
- [35] J. P. B. Silva *et al.*, "Large ferro–pyro–phototronic effect in 0.5Ba(Zr0.2Ti0.8)O3–0.5(Ba0.7Ca0.3)TiO3 thin films integrated on silicon for photodetection," *Carbon Energy*, vol. 5, no. 6, p. e297, 2023, doi: <https://doi.org/10.1002/cey2.297>.
- [36] Z. Liu, H. Wu, W. Ren, and Z.-G. Ye, "4.05 - Piezoelectric and ferroelectric materials: Fundamentals, recent progress, and applications," J. Reedijk and K. R. B. T.-C. I. C. I. I. I. (Third E. Poepelmeier, Eds. Oxford: Elsevier, 2023, pp. 135–171. doi: <https://doi.org/10.1016/B978-0-12-823144-9.00069-8>.
- [37] S. Dwivedi, T. Pareek, and S. Kumar, "Structure, dielectric, and piezoelectric properties of K0.5Na0.5NbO3-based lead-free ceramics," *RSC Adv.*, vol. 8, no. 43, pp. 24286–24296, 2018, doi: 10.1039/C8RA04038A.
- [38] S. Manotham, P. Jaita, P. Butnoi, N. Lertcumfu, and G. Rujijanagul, "Improvements of

- depolarization temperature, piezoelectric and energy harvesting properties of BNT-based ceramics by doping an interstitial dopant," *J. Alloys Compd.*, vol. 897, p. 163021, 2022, doi: <https://doi.org/10.1016/j.jallcom.2021.163021>.
- [39] M. Maraj, W. Wei, B. Peng, and W. Sun, "Dielectric and Energy Storage Properties of  $Ba(1-x)Ca_xZr_yTi(1-y)O_3$  (BCZT): A Review," *Materials*, vol. 12, no. 21, 2019. doi: 10.3390/ma12213641.
- [40] L. Liu, X. Guo, and C. Lee, "Promoting smart cities into the 5G era with multi-field Internet of Things (IoT) applications powered with advanced mechanical energy harvesters," *Nano Energy*, vol. 88, p. 106304, 2021, doi: <https://doi.org/10.1016/j.nanoen.2021.106304>.
- [41] D. Han, W.-T. Chiu, M. Tahara, V. Chernenko, S. Lanceros-Mendez, and H. Hosoda, "Framework of magnetostrain responsive Ni–Mn–Ga microparticles driving magnetic field induced out-of-plane actuation of laminate composite," *Sci. Rep.*, vol. 13, no. 1, p. 7160, 2023, doi: 10.1038/s41598-023-33945-y.
- [42] J. Gou *et al.*, "Large and sensitive magnetostriction in ferromagnetic composites with nanodispersive precipitates," *NPG Asia Mater.*, vol. 13, no. 1, p. 6, 2021, doi: 10.1038/s41427-020-00276-7.
- [43] V. Bayzi Isfahani *et al.*, "Flexible Magnetocaloric Fiber Mats for Room-Temperature Energy Applications," *ACS Appl. Mater. Interfaces*, vol. 16, no. 7, pp. 8655–8667, Feb. 2024, doi: 10.1021/acsami.3c15833.
- [44] A. Baghizadeh *et al.*, "Interplay of Magnetic Properties and Doping in Epitaxial Films of h-REFeO<sub>3</sub> Multiferroic Oxides," *Small*, vol. 17, no. 11, p. 2005700, 2021, doi: <https://doi.org/10.1002/smll.202005700>.
- [45] M. Ashfold, F. Claeysens, G. Fuge, and S. Henley, "Pulsed Laser Ablation and Deposition of Thin Films," *Chem. Soc. Rev.*, vol. 33, pp. 23–31, Feb. 2004, doi: 10.1039/b207644f.
- [46] C. Phipps, *Laser Ablation and Its Applications*, vol. 129, 2007. doi: 10.1007/978-0-387-30453-3.
- [47] T. J. Jackson and S. B. Palmer, "Oxide superconductor and magnetic metal thin film deposition by pulsed laser ablation: a review," *J. Phys. D: Appl. Phys.*, vol. 27, no. 8, p. 1581, 1994, doi: 10.1088/0022-3727/27/8/001.
- [48] L. W. Martin, Y.-H. Chu, and R. Ramesh, "Advances in the growth and characterization of magnetic, ferroelectric, and multiferroic oxide thin films," *Mater. Sci. Eng. R Reports*, vol. 68, no. 4, pp. 89–133, 2010, doi: <https://doi.org/10.1016/j.mser.2010.03.001>.
- [49] R. K. Singh, O. W. Holland, and J. Narayan, "Theoretical model for deposition of superconducting thin films using pulsed laser evaporation technique," vol. 68:1, 1990, doi: 10.1063/1.347123.
- [50] J. Schou, S. Amoruso, and J. G. Lunney, "Plume Dynamics of Laser Ablation and its Applications," C. Phipps, Ed. Boston, MA: Springer US, 2007, pp. 67–95. doi: 10.1007/978-0-

387-30453-3\_4.

- [51] J. Schou, "Physical aspects of the pulsed laser deposition technique: The stoichiometric transfer of material from target to film," *Appl. Surf. Sci.*, vol. 255, no. 10, pp. 5191–5198, 2009, doi: <https://doi.org/10.1016/j.apsusc.2008.10.101>.
- [52] K. Reichelt, "Nucleation and growth of thin films," *Vacuum*, vol. 38, no. 12, pp. 1083–1099, 1988, doi: [https://doi.org/10.1016/0042-207X\(88\)90004-8](https://doi.org/10.1016/0042-207X(88)90004-8).
- [53] M. Ohring, "The Material Science of Thin Films," *Mater. Sci. Thin Film.*, pp. 1–704, Jan. 2013.
- [54] F. Rossi, "FUNDAMENTALS IN ION ASSISTED DEPOSITION OF THIN FILMS," 1996.